Composites Science and Technology 72 (2012) 1989–1994

Contents lists available at SciVerse ScienceDirect

Composites Science and Technology

journal homepage: www.elsevier.com/locate/compscitech

# Indentation of functionally graded beams and its application to low-velocity impact response

V.K. Yalamanchili, B.V. Sankar *

*Mechanical & Aerospace Engineering, University of Florida, Gainesville, FL 32611, USA*

ARTICLE INFO

*Article history:*
Received 9 March 2012
Received in revised form 10 August 2012
Accepted 4 September 2012
Available online 13 September 2012

*Keywords:*
A. Hybrid composites
B. Impact behavior
B. Delamination
C. Modeling
C. Elastic properties

ABSTRACT

The problem of contact between a rigid cylindrical indenter and a functionally graded (FG) beam is studied. The elastic modulus of the material varies in an exponential fashion across the thickness of the beam. For the sake of comparison indentation of a homogeneous beam is also considered. In the case of FG beams indentation of both soft and hard sides of the beam are studied. Results are presented for contact force–contact length relations and contact stresses in the three types of beams. Maximum normal strains and stresses and maximum transverse shear stresses are plotted as a function of strain energy (work done by the indenter) in the beam. The results are extended to low-velocity impact problems. It is seen that for a given impact energy in low-velocity impacts, the maximum stresses and strains are significantly lower in FG beams when the impact occurs on the softer side of the beam.



## 1. Introduction

Low-velocity foreign object impact damage is a serious problem in composite materials used in military and civil structures [1,2]. Laminated fiber composites are strong and stiff in the plane of fibers; however they are prone to delamination under impact loads. Attempts have been made to increase impact damage tolerance by using toughened resins and translaminar reinforcements such as Z-pinning and stitching [3,4]. Recently there is a renewed interest in using three-dimensional woven composites in impact critical structures [5–10]. All of the above methods focus on impact damage tolerance and they do not increase impact damage resistance, which is measured by the energy at which damage initiates under impact. Recent advances in textile manufacturing processes allow mixing different fibers to produce composites with varying stiffness and strength properties [11,12]. Now it is possible to create a functionally graded material (FGM) that could be optimized to provide good structural stiffness for the given applications and at the same time provide improved impact damage resistance.

FGMs have been studied extensively for the past 20 years mostly for thermal barrier coatings [13–15]. Contact problems for FGMs have been studied in the context of micro- and nano-indentation techniques used to characterize the material gradation [16,17]. Inverse methods are used to extract the material properties from indentation test results in conjunction with finite element analysis. There are not many works dealing with the impact response of structures made of FGMs. Gong et al. [18], studied the low-velocity impact of a functionally graded cylindrical shell. The contact stiffness was assumed to be a function of the properties of the outermost layer based on their earlier work [19]. Etemadi et al. [20] performed 3D finite element analyses of impact of sandwich beams with functionally graded cores. Since they used 3D FEA, the contact problem could be modeled directly without resorting to approximate contact laws. Apetre et al. [21] developed a model to analyze sandwich plates with FG cores and used that to study the low-velocity impact problem [22]. The contact problem was solved using assumed contact stress method [23]. In this paper we describe the contact problem of a rigid cylinder and a FG beam. Numerous past studies, both experimental and analytical, have demonstrated the relevance of static contact problems to low-velocity impact response [24–28]. The main idea here is that contact force–contact length and contact force–indentation relations are almost the same in the static and dynamic problems as the wave propagation effects are not significant in low-velocity impact. Similarly the stresses in the vicinity of contact are also the same leading to similar damage patterns both in quasi-static and dynamic impact events [26]. Thus the impact damage resistance can be characterized by performing static indentation tests or static contact analysis.

## 2. Problem statement

Consider the beam shown in Fig. 1. Note that the $x$-axis is along the bottom of the beam, not in the mid-plane. The length of the beam is $L$ and depth is $h$. The beam is assumed to be in a state of plane strain

* Corresponding author. Tel.: +1 352 392 6749; fax: +1 352 392 7303.
*E-mail address:* Sankar@ufl.edu (B.V. Sankar).

0266-3538/$ - see front matter © 2012 Elsevier Ltd. All rights reserved.
http://dx.doi.org/10.1016/j.compscitech.2012.09.002

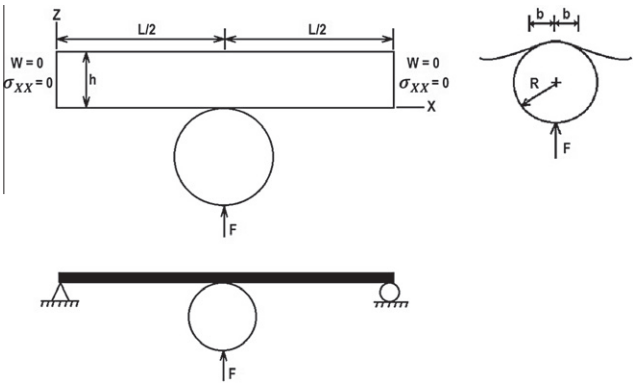


**Fig. 1.** A functionally graded beam indented by a rigid indenter. The elasticity boundary conditions are shown in the top figure. Boundary conditions in the context of beam theory are depicted in the bottom figure.

normal to the $x$–$z$ plane, and the width in the $y$-direction is taken as unity. The boundary conditions are similar to that of a simply supported beam in the context of beam theory, but the exact boundary conditions will become apparent later. The material is assumed to be isotropic at every point and the Poisson's ratio is assumed to be a constant. The Young's modulus varies exponentially in the $z$-direction, and the variation is given by $E(z) = E_0 e^{\lambda z}$ where $\lambda$ determines the degree of gradation of the material properties in the $z$-direction. The beam is indented by a smooth cylinder of radius $R$ at the center of the beam on the bottom face (Fig. 1). Our goal is to determine a relationship between the contact force $F$ and the contact length $2b$, and also the detailed stress field in the beam for a given contact force. The overarching goal of the paper is to understand the effects of various types of gradation of material properties on the stress field, especially in the vicinity of contact.

The governing equations of the problem are the two stress equilibrium equations:

$$\frac{\partial \sigma_{xx}}{\partial x} + \frac{\partial \tau_{xz}}{\partial z} = 0, \quad \frac{\partial \tau_{xz}}{\partial x} + \frac{\partial \sigma_{zz}}{\partial z} = 0 \tag{1}$$

The constitutive relations are given by

$$\begin{Bmatrix} \sigma_{xx} \\ \sigma_{zz} \\ \tau_{xz} \end{Bmatrix} = \begin{bmatrix} C_{11} & C_{13} & 0 \\ C_{13} & C_{33} & 0 \\ 0 & 0 & C_{55} \end{bmatrix} \begin{Bmatrix} \varepsilon_{xx} \\ \varepsilon_{zz} \\ \gamma_{xz} \end{Bmatrix} \quad \text{or} \quad \{\sigma\} = [C(z)]\{\varepsilon\} \tag{2}$$

The stiffness coefficients $C_{ij}$ will also vary as $C_{ij}(z) = C_{ij}(0)e^{\lambda z}$. For the case of plane strain considered in this study $C_{ij}$ are related to $E$ and $v$ by

$$C_{11} = C_{33} = \frac{E(1-v)}{(1+v)(1-2v)}, \quad C_{13} = \frac{Ev}{(1+v)(1-2v)}, \quad C_{55} = \frac{E}{2(1+v)} \tag{3}$$

Substituting the stress–strain relations (2) into the equilibrium Eq. (1) and using the strain displacement relations $\varepsilon_{xx} = \frac{\partial u}{\partial x}$, $\varepsilon_{yy} = \frac{\partial v}{\partial y}$ and $\gamma_{xy} = \frac{\partial u}{\partial y} + \frac{\partial v}{\partial x}$ the governing differential equations of the problem are obtained as

$$\begin{aligned} &\frac{\partial}{\partial x}\left(C_{11}\frac{\partial u}{\partial x} + C_{13}\frac{\partial w}{\partial z}\right) + \frac{\partial}{\partial z}\left(C_{55}\frac{\partial u}{\partial z} + C_{55}\frac{\partial w}{\partial x}\right) = 0 \\ &\frac{\partial}{\partial x}\left(C_{55}\frac{\partial u}{\partial z} + C_{55}\frac{\partial w}{\partial x}\right) + \frac{\partial}{\partial z}\left(C_{13}\frac{\partial u}{\partial x} + C_{33}\frac{\partial w}{\partial z}\right) = 0 \end{aligned} \tag{4}$$

The boundary conditions on the left and right ends of the beam ($x = 0$ and $x = L$) are:

$$\begin{aligned} &w(0,z) = w(L,z) = 0 \\ &\sigma_{xx}(0,z) = \sigma_{xx}(L,z) = 0 \end{aligned} \tag{5}$$

One can note that the above BCs are similar to that of a simply supported beam in the context of beam theory for slender beams, i.e., $L \gg h$.

The top surface of the beam ($z = h$) is traction free:

$$\sigma_{zz}(x,h) = \tau_{xz}(x,h) = 0 \tag{6}$$

On the bottom surface ($z = 0$) we have mixed boundary conditions: the shear stress $\tau_{xz}$ vanishes everywhere on the bottom surface; the normal stress $\sigma_{zz} = 0$ outside the contact region; and in the contact region the $w$-displacements should be such that the deformed surface conforms to the shape of the rigid indenter. The above BCs can be written as;

$$\tau_{xz}\ (x,0) = 0 \tag{7}$$

$$\sigma_{zz}(x,0) = 0, \quad |\chi| > b, \qquad \chi = x - L/2 \ \text{(outside the contact region)} \tag{8}$$

$$w(x,0) = \Delta - \frac{\chi^2}{2R}, \quad |\chi| \leqslant b \ \text{(inside the contact region)} \tag{9}$$

where $\Delta$ is the indenter displacement in the $z$-direction, and $2b$ is the contact length (see Fig. 1). Note that we have introduced the variable $\chi = (x - L/2)$ to facilitate easy discussion of the contact problem. The point $\chi = 0$ corresponds to the center of the beam. The profile of the indenter in the vicinity of contact is approximated as a parabola as shown in (9) which is valid only when the contact length $b$ is much smaller than the indenter radius $R$.

The contact problem will be solved using an assumed contact stress approach. The contact stresses are assumed of the form

$$p_z(x) = -\sigma_{zz}(x,0) = \sum_{i=1}^{N} p_i \phi_i(x), \quad |\chi| \leqslant b \tag{10}$$

where $\phi_i$ are known functions of $x$, and $p_i$ are coefficients to be determined such that they satisfy the contact condition (9). Noting that $w(L/2,0) = \Delta$, the contact condition can be written as

$$w\left(\frac{L}{2},0\right) - w(x,0) = \frac{\chi^2}{2R}, \quad |\chi| \leqslant b \ \text{(inside the contact region)} \tag{11}$$

A collocation method will be used to solve for $p_i$. In this method the above contact condition is satisfied at $M$ number of discrete points $x = x_j$ on the contact surface:

$$w\left(\frac{L}{2},0\right) - w(x_j,0) = \frac{\chi_j^2}{2R}, \quad |\chi_j| \leqslant b \quad (j = 1, M;\ M \geqslant N) \tag{12}$$

where $\chi_j = (x_j - L/2)$. Note that $M$ should be at least equal to $N$, but it is found that matching the displacements at more number of points improves the accuracy of the solution for contact stresses [29]. Past studies show that equally spaced collocation points yield good results [30,31]. The surface displacements $w$ can be written as linear combination of the unknown pressure coefficients $p_i$:

$$\sum_{i=1}^{N} (c_{0i} - c_{ji}) p_i = \frac{\chi_j^2}{2R} \quad (j = 1, M;\ M \geqslant N) \tag{13}$$

where $c_{0i}$ is the central displacement $w(L/2,0)$ and $c_{ji}$ is equal to displacement $w(x_j,0)$ at $x_j$ due to unit $p_i$. The over determined system of linear equations (13) can be solved for $p_i$ using the least square error procedure.

The elasticity problem of an FG beam with the BCs given in Eq. (5) and subjected to an arbitrary loading $p_z(x)$ was solved using Fourier transforms in [29]. In this work procedures are described for calculating the displacement field $u(x,z)$ and $w(x,z)$. The same procedures can be used to determine the influence coefficients $c_{0i}$

and $c_{ji}$. In the following we give a brief description of the method.Our goal is to solve the pair of partial differential Eq. (4) subjected to the boundary conditions (5) and (6). We will solve the problem for the case $p_z(x) = q_n \sin \xi x$ where $\xi = n\pi x/L$. The displacements are assumed of the form

$$\begin{aligned} u(x,z) &= U(z)\cos\xi x \\ w(x,z) &= W(z)\sin\xi x \end{aligned} \tag{14}$$

Substituting the above displacements in the governing differential Eq. (4) we obtain a pair of ordinary differential equations (ODEs) for $U(z)$ and $W(z)$ which are solved using the solution of the form

$$\begin{aligned} U(z) &= \sum_{i=1}^{4} a_i e^{\alpha_i z} \\ W(z) &= \sum_{i=1}^{4} b_i e^{\alpha_i z} \end{aligned} \tag{15}$$

where $\alpha_i$ are roots of the characteristic equation associated with the ODEs. The arbitrary constants $a_i$ and $b_i$ are solved using the stress boundary conditions on the top surface of the beam given by (6), and stress BCs on the bottom of the beam as given below:

$$\begin{aligned} \tau_{zx}(x,0) &= 0 \\ \sigma_{zz}(x,0) &= -p_z(x) = -q_n \sin\xi x \end{aligned} \tag{16}$$

Once constants $a_i$ and $b_i$ are evaluated, the displacement field $u$ and $v$ are completely determined, and the strains and stresses at any point can be calculated using the strain–displacement relations and constitutive relations. For more details on the procedures the reader is referred to [29].

## 3. Contact problem

### 3.1. Assumed contact stress distribution method

In this method [30,31] the contact is approximated as Hertzian contact (elliptical contact stress distribution), and a one-term function for (10) is used as

$$p_z(x) = p_m \sqrt{1 - \left(\frac{\chi}{b}\right)^2}, \quad |\chi| < b \tag{17}$$

Thus $p_m$, the peak contact stress, is the only unknown. Then, Eq. (13) to determine $p_m$ takes the form

$$p_m(c_0 - c_j) = \frac{\chi_j^2}{2R} \quad (j = 1, M;\ M \geqslant 1) \tag{18}$$

where $c_0$ is the $w$-displacement at the center ($x = L/2$, $z = 0$) and $c_j$ are the $w$-displacements at $x_j$ due to the elliptical contact load with $p_m = 1$. The least square error solution of the above equation is

$$p_m = \frac{1}{M}\sum_{j=1}^{M} \frac{\chi_j^2}{2R(c_0 - c_j)} \tag{19}$$

The influence coefficients $c_0$ and $c_j$ can be calculated for $p_z(x) = \sqrt{1 - \left(\frac{\chi}{b}\right)^2}$ using the procedures described in [29]. That method uses Fourier transforms to solve the elasticity equations and load $p_z$ has to be expanded in the form of a Fourier series

$$p_z(x) = \sum_{n=1}^{\infty} q_n \sin\frac{n\pi}{L}x \tag{20}$$

where the Fourier coefficients are given by

$$q_n = \frac{2}{L}\int_0^L p_z(x)\sin\frac{n\pi x}{L}\,dx \tag{21}$$

For the case of Hertzian contact stress above the Fourier coefficients can be derived as

$$\begin{aligned} q_n &= \tfrac{2p_m}{L}\int_0^L \sqrt{1-\left(\tfrac{\chi}{b}\right)^2}\sin\tfrac{n\pi x}{L}dx \\ &= \tfrac{2(-1)^{\frac{n-1}{2}}p_m}{L}\int_{-b}^{+b}\sqrt{1-\left(\tfrac{\chi}{b}\right)^2}\cos\tfrac{n\pi\chi}{L}d\chi,\ (n=1,3,5\ldots) \\ &= \tfrac{2(-1)^{\frac{n-1}{2}}p_m}{n}J_1\left(\tfrac{n\pi b}{L}\right) \end{aligned} \tag{22}$$

where $J_1$ is the Bessel function of the first kind. In evaluating the above we have used the relation

$$\int_{-c}^{c}\sqrt{c^2 - x^2}\cos\xi x\,dx = \frac{\pi c}{\xi}J_1(c\xi) \tag{23}$$

### 3.2. Application to low-velocity Impact

The first step in solving a low-velocity foreign object impact problem is to obtain the impact force history [25]. Numerous past studies [24,26] – both experimental and analytical – have shown that the load–deflection relation in low velocity impacts could be approximated by corresponding static load–deflection relations. Furthermore, the contact force–contact width ($F$–$b$) relations also follow the corresponding quasi-static relations. This fact has been used to simplify analysis of low velocity impact response and damage of composite structures. Then the maximum impact force can be related to the initial impact energy as

$$U = \frac{1}{2}m_i v_i^2 = \frac{1}{2}\frac{F_m^2}{k_b} \tag{24}$$

where the impact energy is the initial kinetic energy of the impacting mass, $F_m$ the maximum impact force, and $k_b$ is the bending stiffness of the beam when a point load is applied at the center. In the above energy relation strain energy due to local indentation in the vicinity of contact is neglected.

## 4. Results and discussion

The dimensions of the beam used in this study are: length $L = 100$ mm and depth $h = 10$ mm. A state of plane strain normal to the $y$-axis is assumed and the width in the $y$-direction is taken as unity. The radius of curvature of the indenter $R$ in the numerical examples is taken as 20 mm. Two types of FG beams and a homogeneous beam are considered. The Young's moduli of the FG beams and the homogeneous beam are given in Table 1. The through-the thickness variation of $E$ is shown in Fig. 2. In Beam 1 the grading parameter $\lambda$ is positive, that is, the Young's modulus increases from 20 to 200 GPa as $z$ increase from 0 to $h$. This case will be designated as soft impact as the beam is indented on the softer side. The value of $\lambda$ for Beam 2 is negative, and the Young's modulus is high at $z = 0$ and decreases towards $z = h$. This case is designated as hard impact. For comparison a homogeneous beam (Beam 3) is also considered. The bending stiffness $k_b$ of all three beams is kept 261 N/mm. The bending stiffness is calculated as

$$k_b = \frac{48D_{11}^*}{L^3} \tag{25}$$

where $D_{11}^*$ is the reduced stiffness [29]. For the homogeneous beam the above relation takes the simple form $k_b = \frac{48Eh^3}{(1-\nu^2)L^3}$.

### 4.1. Contact force–contact length ($F$–$b$) relations and contact stresses

The contact force–half contact length ($F$–$b$) relations are shown in Fig. 3 for all three beams. In the same plot the Hertzian relations for a half-plane for the three beams are given. The Hertzian relation for a homogeneous half-plane under plane strain is given by [30] $F = \frac{\pi\bar{E}}{4R}b^2$ where $\bar{E} = E/(1-\nu^2)$. In Fig. 3 the Hertzian plots for the two graded beams are based on the Young's modulus $E(0)$ on the contacting surface. One can note that for small contact lengths

**Table 1**
Properties of the three materials used in the present study.

| | | $E_0$ (GPa) | $E_h$ (GPa) | Grading parameter $\lambda$ ($m^{-1}$) | Poisson's ratio $v$ | Bending stiffness $k_b$ (N/mm) |
|---|---|---|---|---|---|---|
| 1 | Functionally graded beam (soft impact) | 20 | 200 | +230 | 0.25 | 261 |
| 2 | Functionally graded beam (hard impact) | 200 | 20 | −230 | 0.25 | 261 |
| 3 | Homogeneous beam | 61.1 | 61.1 | 0 | 0.25 | 261 |

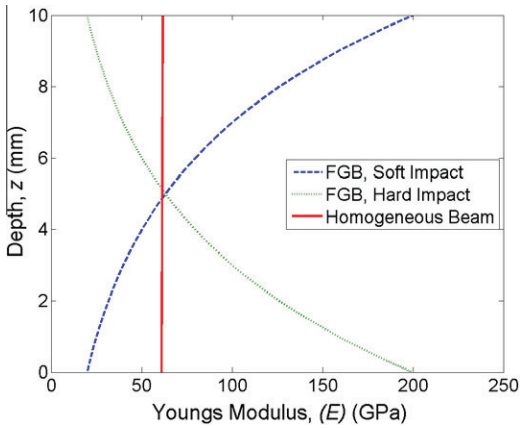


**Fig. 2.** Variation of Young's modulus through the thickness of three different beams considered.

the $F$–$b$ relation for a homogeneous beam agrees well with that of the corresponding half-plane. As the contact force increases the contact length in the homogeneous beam becomes slightly larger than that in the half-plane. This is due to the finite curvature of the deformed beam, and the contact relation can be modified to account for the finite curvature of the beam ($\kappa_{\text{beam}}$) as discussed in [30,31]. The present numerical solution agrees well with the corrected $F$–$b$ relation for the homogenous beam as shown in Fig. 3.

In the case of FG beams we observe the following: first we will consider the hard impact case wherein $E$ varies from a higher value on the contacting surface to a lower value inside the beam. For small contact force, the contact length is slightly larger than the corresponding Hertzian result as the indenter begins to see the soft material ahead of the contact region. As the load is increases aforementioned curvature effect also comes into play increasing the contact length further, and the $F$–$b$ relation deviates considerably from the Hertzian result based on the surface Young's modulus.

The reverse is true for soft impact wherein the Young's modulus increases from a smaller value at the contact surface to a larger value inside the beam. In the beginning the contact length is slightly smaller than the Hertzian result. This is again because the indenter senses the stiffer material ahead of the contact region. As the force is increased the rate of increase of contact length should decrease because of the stiffer material ahead. However, the curvature effect comes into play, which tends to increase the contact length. Thus the two effects seem to nullify each other and the $F$–$b$ relation follows the power law for considerable amount of contact force, even better than the homogeneous beam.

The contact stress distribution ($-\sigma_{zz}(x)$ vs. $\chi$) for the three types of beam are presented in Fig. 4. Due to symmetry only one half of the distribution for $0 < \chi/b < 1$ is shown. The results shown in Fig. 4 for contact length $b = 2.5$ mm ($b/R = 0.125$ or $b/h = 0.25$). Obviously the peak stress is proportional to the contact force which, for a given contact length, is the highest for the hard impact case and the lowest for the soft impact case (also see Fig. 3).

### 4.2. Stress field

The variation of bending stress $\sigma_{xx}(L/2,z)$ at the center of the beam (below the indenter) at $x = L/2$ is shown in Fig. 5. The results reveal no surprises and they are similar to that discussed for a general loading in Ref. [29]. The bending stress varies linearly in the homogeneous beam except in the vicinity of contact. The nonlinear variation of stresses in the FG beams is mainly due to the variation of $E$ through the thickness. The stress concentration in the vicinity of contact is more pronounced in the hard impact case. Sample normalized transverse shear stress distribution, $\tau_{xz}(z)$, across the beam height are shown in Fig. 6 for a cross section in the vicinity of contact ($x = L/2 + b$), and in Fig. 7 for a cross section away from contact ($x = 3L/4$). The shear stresses are normalized by the average shear stress, $F/h$. One can see the typical shear stress concentration near the contact surface (Fig. 6). These maximum shear stresses are responsible for damage initiation due to low-velocity impact. The shear stress concentration is much higher in hard contact case. The shear stresses away from contact (Fig. 7) are similar to that in homogeneous (parabolic variation) and FG beams reported earlier [29].

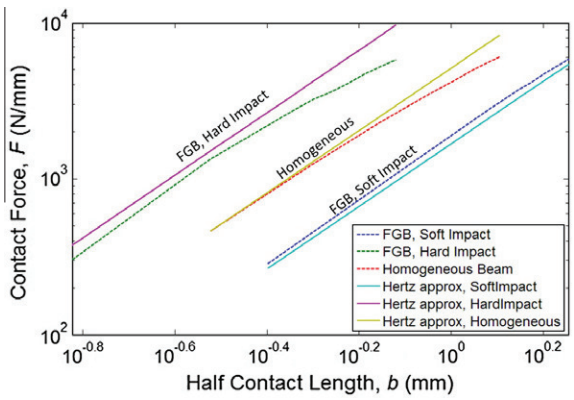


**Fig. 3.** Logarithmic plot of contact force–contact length relations for various beams. For FG beams Hertzian approximations are based on the Young's modulus of the material at the contacting surface.

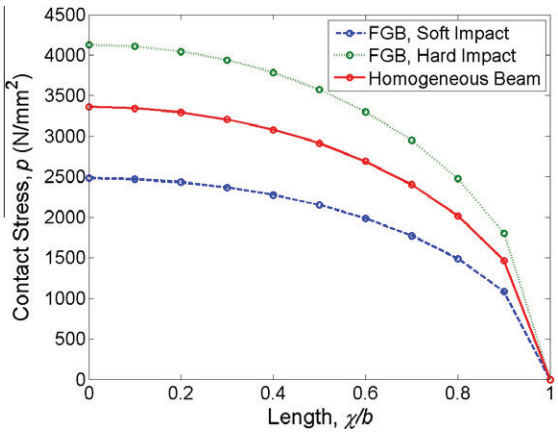


**Fig. 4.** Contact stress distribution in the three beams for $b = 2.5$ mm ($b/R = 0.125$ or $b/h = 0.25$).

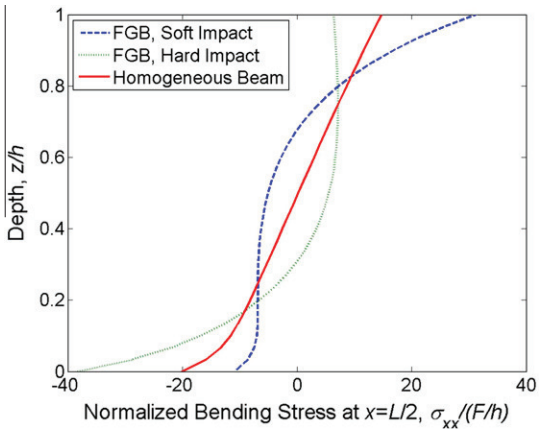


**Fig. 5.** An example of variation of bending stresses through the thickness.

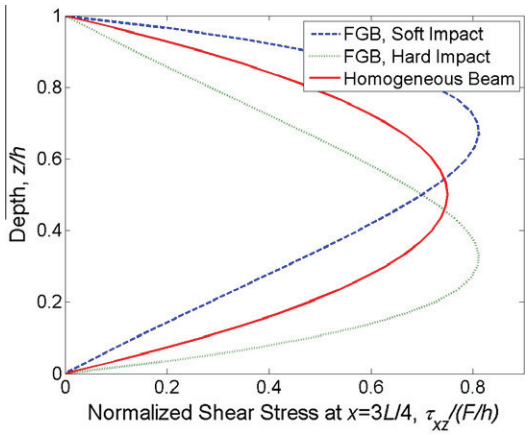


**Fig. 7.** Transverse shear stress at a cross section away from contact. Note the typical parabolic profile in the homogeneous beam and slight deviations from that in FG beams.

### 4.3. Maximum stresses and strains

One of the goals of this paper is to explore the possibility of using functionally graded materials to reduce impact damage. Hence, we would like to compare maximum stresses and strains in various beams for a given impact energy. However, we do not have knowledge of strength or allowable stresses for FG materials. They will vary from point to point as the Young's modulus varies. Hence, it would be reasonable to look at maximum strains rather than maximum stresses. Maximum strains were calculated from the strain values in the entire beam and they are the global maximum. The maximum principal strain in the beam is plotted in Fig. 8 as a function of impact energy. The maximum shear strain is plotted in Fig. 9. From Fig. 8 it is clear that the maximum principal strain is much less in soft impact, that is, when the FG beam is positioned such way the impact occurs on the softer side. The maximum strain is the largest in hard impact and the homogeneous beam's performance is somewhere in between. We look at maximum strain as it is expected to govern failure in brittle materials. If the material is ductile, then one might look into maximum shear strain for the purpose of comparison. If maximum shear strain is considered (Fig. 9), homogeneous beam has the best performance. The maximum shear strain in the homogeneous beam is less than that in the two FG beams. Within the two FG beams the softer impact produces less maximum shear strain.

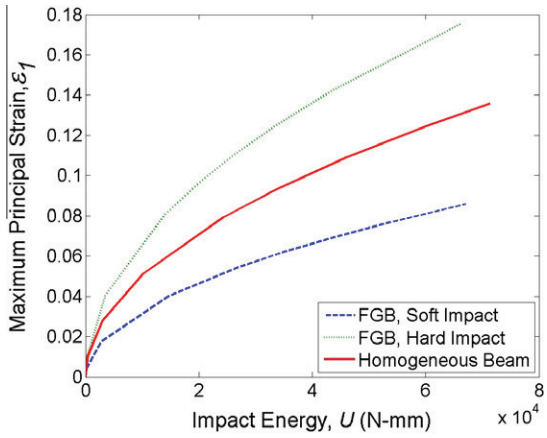


**Fig. 8.** Maximum principal strain in the three beams as a function of impact energy.

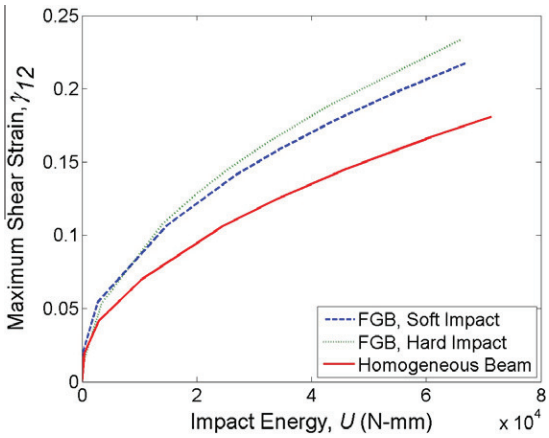


**Fig. 9.** Maximum shear strain in the three beams as a function of impact energy.

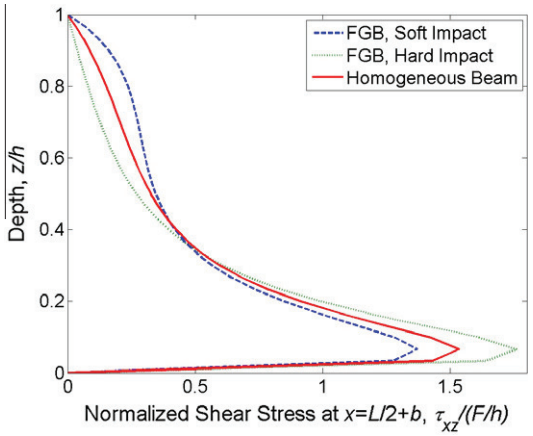


**Fig. 6.** Transverse shear stresses at a cross section in the vicinity of contact. The results are for $b = 1$ mm.

### 4.4. Interlaminar shear stresses

Lamination or layering is still the popular process for making beam/plate like composite structures. If the FG beams are fabricated using the lamination process, then the interlaminar shear stress (ILS) $\tau_{zx}$, which is also equal to the transverse shear stress $\tau_{xz}$, will play a role in determining the integrity of the lamination

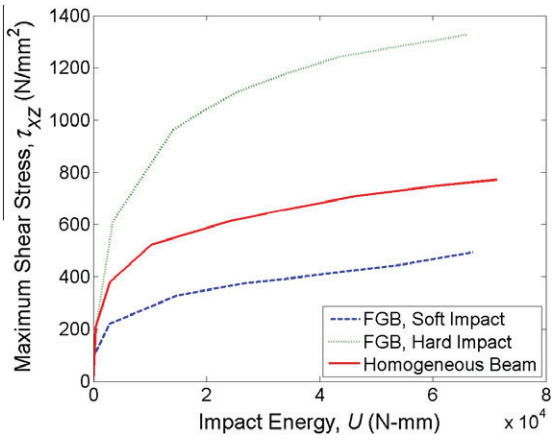


**Fig. 10.** Maximum interlaminar shear stress in the three beams as a function of impact energy.

process. The maximum interlaminar shear stress as a function of impact energy is plotted for the three types of beams in Fig. 10. Again the maximum stresses presented are the global maximum. It can be seen that for a given impact energy the ILS is much lower in soft impact compared to the other two cases. That means, for a given interlaminar shear strength, the beam can take higher impact load in soft impact.

## 5. Summary and conclusions

The problem of smooth indentation of a beam made of functionally graded material is studied. Two types of gradations – soft to hard and hard to soft – and a homogeneous material were studied. The flexural stiffness of the three beams was kept the same. For small contact force the Hertzian semi-elliptical contact stress distribution seems to be a reasonable approximation. However, variation of Young's modulus in FG beams has a significant effect on the contact length. In addition, the finite curvature of the beam also tends to increase the contact length.

For a given contact force the contact length in soft contact is about three times that in hard contact. This reduces the peak contact stress which in turn seems to reduce the stresses in the contact region. It is found that for a given impact energy or a given maximum contact force, maximum normal and shear strains were in general less in soft impact, i.e., when the impact/contact occurred on the softer side. This is especially true for interlaminar shear stresses, which may play a role in the design of laminated FG beams.

## Acknowledgements

The funding for this work was provided by the United States Army Research Office (Grant Number W911NF-08-1-0120) and the United States Army Research Laboratory (ARL) at Aberdeen Proving Ground, MD. The authors appreciate the support and encouragement of Dr. Chian-Fong Yen of ARL.

## References

[1] Lewis SJ. The use of carbon fibre composites on military aircraft. Compos Manuf 1994;5(2):95–103.
[2] Fink BK. Performance metrics for composite integral armor. J Thermoplast Compos Mater 2000;13(5):417–31.
[3] Sankar BV, Zhu H. Effect of stitching on the low-velocity impact response of delaminated composite beams. Compos Sci Technol 2000;60:2681–91.
[4] Sharma SK, Sankar BV. Effect of stitching on impact and interlaminar properties of graphite/epoxy laminates. J Thermoplast Compos Mater 1997;10(3):241–53.
[5] Walter TR, Subhash G, Sankar BV, Yen CF. Monotonic and cyclic short beam shear response of 3D woven composites. Compos Sci Technol 2010;70:2190–7.
[6] Walter TR, Subhash G, Sankar BV, Yen CF. Damage modes in 3D glass fiber epoxy woven composites under high rate of impact loading. Composites Part B 2009;40:584–9.
[7] Rao MP, Sankar BV, Subhash G. Effect of Z-yarns on the stiffness and strength of three-dimensional woven composites. Composites Part B 2009;40:540–51.
[8] Pankow M, Salvi A, Waas AM, Yen CF, Ghiorse S. Resistance to delamination of 3D woven textile composites evaluated using end notch flexure (ENF) tests experimental results. Composites Part A 2011;42:1463–76.
[9] Pankow M, Waas AM, Yen CF, Ghiorse S. Resistance to delamination of 3D woven textile composites evaluated using End Notch Flexure (ENF) tests: Cohesive zone based computational results. Composites Part A 2011;42(12):1863–72.
[10] Gong JC, Sankar BV. Impact properties of three-dimensional braided graphite/epoxy composites. J Compos Mater 1991;25(6):715–31.
[11] Hosur MV, Adbullah M, Jeelani S. Studies on the low-velocity impact response of woven hybrid composites. Compos Struct 2005;67(3):253–62.
[12] Gustin J, Joneson A, Mahinfalah M, Stone J. Low velocity impact of combination Kevlar/carbon fiber sandwich composites. Compos Struct 2005;69(4):4396–406.
[13] Suresh S, Mortensen A. Fundamentals of functionally graded materials. London: IOM Communications Limited; 1995.
[14] Rangaraj S, Kokini K. Estimating the fracture resistance of functionally graded thermal barrier coatings from thermal shock tests. Surf Coat Technol 2003;173(2–3):201–12.
[15] Kawasaki A, Watanabe R. Thermal fracture behavior of metal/ceramic functionally graded materials. Eng Fract Mech 2002;69(14–16):1713–28.
[16] Nakamura T, Wang T, Sampath S. Determination of properties of graded materials by inverse analysis and instrumented indentation. Acta Mater 2000;48:4293–306.
[17] Guler MA, Erdogan F. Contact mechanics of graded coatings. Int J Solids Struct 2004;41(14):3865–89.
[18] Gong SW, Lam KY, Reddy JN. The elastic response of functionally graded cylindrical shells to low-velocity impact. Int J Impact Eng 1999;22:397–417.
[19] Gong SW, Toh SL, Shim VPM. The elastic response of orthotropic laminated cylindrical shells to low velocity impact. Compos Eng 1994;4(2):247–66.
[20] Etemadi E, Khatibi AA, Takaffoli M. 3D finite element simulation of sandwich panels with a functionally graded core subjected to low velocity impact. Compos Struct 2009;89:28–34.
[21] Apetre NA, Sankar BV, Ambur DR. Analytical modeling of sandwich beams with functionally graded core. J Sandwich Struct Mater 2008;10(1):53–74.
[22] Apetre NA, Sankar BV, Ambur DR. Low-velocity impact response of sandwich beams with functionally graded core. Int J Solids Struct 2006;43:2479–96.
[23] Sankar BV, Sun CT. Indentation of a beam by a rigid cylinder. Int J Solids Struct 1983;19(4):293–303.
[24] Tan TM, Sun CT. Use of statical indentation laws in the impact analysis of laminated composite plates. J Appl Mech 1985;52(1):6–12.
[25] Sankar BV, Sun CT. An efficient numerical algorithm for transverse impact problems. Comput Struct 1985;20(6):1009–12.
[26] Kwon YS, Sankar BV. Indentation-flexure and low-velocity impact damage in graphite/epoxy laminates. ASTM J Compos Technol Res 1993;15(2):101–11.
[27] Sankar BV, Sun CT. Low-velocity impact response of laminated beams subjected to initial stresses. AIAA J 1985;23(12):1962–9.
[28] Sankar BV. Scaling of low-velocity impact for symmetric laminates. J Reinf Plast Compos 1992;11(3):296–309.
[29] Sankar BV. An elasticity solution for functionally graded beams. Compos Sci Technol 2001;61:689–96.
[30] Sankar BV. Smooth indentation of orthotropic beams. Compos Sci Technol 1989;34(2):95–111.
[31] Sankar BV. An integral equation for the problem of smooth indentation of orthotropic beams. Int J Solids Struct 1989;25(3):327–37.